
Article:
Palanca, M. orcid.org/0000-0002-1231-2728, Barbanti-Bròdano, G., Marras, D. et al. (5 more authors) (2021) Type, size, and position of metastatic lesions explain the deformation of the vertebrae under complex loading conditions. Bone, 151. 116028. ISSN 8756-3282

https://doi.org/10.1016/j.bone.2021.116028

Bone 151 (2021) 116028

Contents lists available at ScienceDirect

Bone

journal homepage: www.elsevier.com/locate/bone

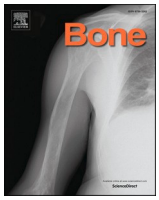

Full Length Article

Type, size, and position of metastatic lesions explain the deformation of the vertebrae under complex loading conditions

Marco Palanca [a,b,*], Giovanni Barbanti-Bròdano [c], Daniele Marras [b], Mara Marciante [b], Michele Serra [b], Alessandro Gasbarrini [c], Enrico Dall'Ara [a], Luca Cristofolini [b]

[a] Dept of Oncology and Metabolism, INSIGNEO Institute for In Silico Medicine, University of Sheffield, Sheffield, UK
[b] Dept of Industrial Engineering, Alma Mater Studiorum – University of Bologna, Bologna, Italy
[c] Dept of Spine Surgery, IRCCS Istituto Ortopedico Rizzoli, Bologna, Italy

ARTICLE INFO

Keywords:
Metastasis
Vertebra
Digital image correlation
Strain analysis

ABSTRACT

Background: Bone metastases may lead to spine instability and increase the risk of fracture. Scoring systems are available to assess critical metastases, but they lack specificity, and provide uncertain indications over a wide range, where most cases fall.
The aim of this work was to use a novel biomechanical approach to evaluate the effect of lesion type, size, and location on the deformation of the metastatic vertebra.
Method: Vertebrae with metastases were identified from 16 human spines from a donation programme. The size and position of the metastases, and the Spine Instability Neoplastic Score (SINS) were evaluated from clinical Quantitative Computed Tomography images. Thirty-five spine segments consisting of metastatic vertebrae and adjacent healthy controls were biomechanically tested in four different loading conditions. The strain distribution over the entire vertebral bodies was measured with Digital Image Correlation. Correlations between the features of the metastasis (type, size, position and SINS) and the deformation of the metastatic vertebrae were statistically explored.
Results: The metastatic type (lytic, blastic, mixed) characterizes the vertebral behaviour (Kruskal-Wallis, $p = 0.04$). In fact, the lytic metastases showed more critical deformation compared to the control vertebrae (average: 2-fold increase, with peaks of 14-fold increase). By contrast, the vertebrae with mixed or blastic metastases did not show a clear trend, with deformations similar or lower than the controls. Once the position of the lytic lesion with respect to the loading direction was taken into account, the size of the lesion was significantly correlated with the perturbation to the strain distribution ($r^2 = 0.72$, $p < 0.001$). Conversely, the SINS poorly correlated with the mechanical evidence, and only in case of lytic lesions ($r^2 = 0.25$, $p < 0.0001$).
Conclusion: These results highlight the relevance of the size and location of the lytic lesion, which are marginally considered in the current clinical scoring systems, in driving the spinal biomechanical instability. The strong correlation with the biomechanical evidence indicates that these parameters are representative of the mechanical competence of the vertebra. The improved explanatory power compared to the SINS suggests including them in future guidelines for the clinical practice.

1. Introduction

Among the neurological, oncologic, mechanical and systemic [1] diseases associated with the spinal metastasis, the evaluation of the spine stability plays a fundamental role due to the possible comorbidities which could be triggered, such as the paralysis of patient. Spine stability is a broad term that indicates the loss of spinal integrity as a result of a neoplastic process [2]. The different types of metastases have different effects on the vertebral mechanics, possibly reducing the load bearing and increasing the risk of fracture [3].

Decision about the spine stabilization is aided by classifications such as the Spine Instability Neoplastic Score (SINS) [2]. The SINS estimates the overall spine stability in case of metastasis considering five objective radiographic criteria (i.e. location of the metastatic vertebra(e) along

* Corresponding author at: Dept of Oncology and Metabolism, INSIGNEO Institute for In Silico Medicine, University of Sheffield, Sheffield, UK.
E-mail addresses: m.palanca@sheffield.ac.uk, marco.palanca@unibo.it (M. Palanca).

https://doi.org/10.1016/j.bone.2021.116028
Received 27 January 2021; Received in revised form 14 May 2021; Accepted 29 May 2021
Available online 2 June 2021

the spine, bone lesion type, radiographic spinal alignment, vertebral body collapse and posterolateral involvement of the spinal elements) and a subjective patient symptom (i.e. the pain associated to movement/loading of the spine). No metastatic features (e.g. size and position) are considered in the SINS. Despite the great inter- and intra-observer reliability [4,5], the SINS has a high grade of uncertainty (indeterminate range of scores: from 7/18 to 12/18), where most cases fall (approximately 60%) [6].

Biomechanical evidences of the metastasis effect were explored with experimental [7–12] and computational [13–19] studies but their outcomes are still not unanimous [20] and they only partially explain the complexity of the problem. While it has been ascertained [21] that the metastases can weaken the bone, the relationship between metastatic features (e.g. size, position, cortical involvement) and their biomechanical consequences are still unclear. This lack of knowledge may be due to the complexity in investigating the biomechanical properties of metastatic spine segments, which comprise soft (intervertebral discs) and hard (vertebrae) tissues, which are difficult to investigate simultaneously, and the complexity in developing highly reproducible testing procedures that could replicate different loading scenarios. The metastatic spine is more frequently characterized considering only the apparent (overall) mechanical properties of the single vertebra, as stiffness and strength [7,12], in a single loading condition. As destructive tests can be performed only once on each specimen, they provide reliable information about the strength only for the selected loading condition. This approach does not provide a comprehensive description of the mechanical behaviour of the vertebra and could hide the local effects induced by the metastasis. Investigating the strain distribution would enable observing the perturbation induced by the different types and sizes of metastasis. Moreover, strength reference values for the metastatic vertebrae were not available, so a different indicator should be used to clearly identify the vertebral behaviour. A full-field strain analysis, indeed, could be used as a surrogate of the vertebral strength [22] and would describe the overall behaviour of such a complex structure, as a result of the local analysis. The Digital Image Correlation (DIC) analysis [23] consists in acquiring images of the specimen, which has to be prepared with a random speckle pattern on the surface, and allows measuring the full-field strains in nearly-real-time on the surface of biological specimens, in a contact-less way, without significantly modifying their mechanical characteristics. The DIC outputs have been validated [24,25] on the vertebrae against strain gauges [26], and they were used to characterize the mechanical properties of healthy [27–30] and damaged vertebra [9,31].

In this study we hypothesize that the features of the metastases, such as the type, the size of the lesion and the position of the lesion with respect to the loading conditions, are determinants of the deformation of the metastatic vertebra. The aim of this study was to evaluate the relationship between the properties of the metastatic lesion (type, size and position) and the deformation of the vertebrae evaluated with full-field surface strain distributions, in different loading conditions.

2. Materials and methods

2.1. Donor details and sample preparation

The study has been approved by the ethical committee of the University of Bologna (n. 17325, 08/02/2019) and the tests were performed in accordance with the Declaration of Helsinki. A batch of 16 spines of active donors with a history of spinal metastasis, derived from different primary tumours (Table 1), were obtained through an ethically approved donation programme (Anatomic Gifts Registry, USA).

Segments of four vertebrae with one healthy (later referred to as "control") and one metastatic vertebra in the middle, or spine segments of five vertebrae, with two consecutive metastatic vertebrae and one control, were prepared (see Supplementary material 1). These configurations were chosen because they allowed us to study control and metastatic vertebrae in each segment, assuming for both vertebrae the same loading conditions during the biomechanical testing. The anterior longitudinal ligaments and the periosteum were removed, in order to expose the cortical bone for the digital image correlation analysis, while the posterior ligaments were left intact. 29 spine segments, for a total of 35 metastatic vertebrae, were extracted. The spine segments were aligned [32] and the two extreme vertebrae were embedded in polymethyl-methacrylate, to be mounted in the testing machine.

2.2. Assessment of the metastasis

The entire spines were scanned with a quantitative computed tomography (qCT) (AquilonOne, Toshiba, Japan) with an optimized bone protocol (voltage: 120 KVp, current: 200 mA, slice thickness: 1 mm, in-plane resolution: around 0.45 mm), in order to localize the vertebrae with metastasis and evaluate their SINS.

After the preparation, previously described, each spine segment was re-scanned, with the same qCT and another protocol, feasible in the clinical practice but with a higher resolution (voltage: 120 KVp, current: 200 mA, slice thickness: 0.5 mm, in-plane resolution: approximately 0.25 mm), in order to better measure the size and assess the position of the metastasis within the vertebra.

Table 1
List of the donors' details.

Donor	Sex	Age	BMI	Primary tumour	Chemotherapy/ radiotherapy	Drug treatment[a]
A	M	81	23	Adrenal	y/y	–
B	M	63	23	Lung	y/y	–
C	F	59	36	Uterine	y/y	–
D	F	51	14	Lung	y/y	Prednisone, Vit D3
E	M	75	17	Bladder	n/n	Decadron
F	F	82	22	Breast	y/y	Letrozole, Prednisone
G	F	55	17	Breast	y/y	Vit D3
H	M	83	21	Prostate	y/n	Apalutamide, Decadron, Degarelix, Denosumab, Lupron, Prednisone, Vit D, Xtandi
I	M	78	16	Prostate	y/y	Deltasone, Denosumab, Lupron, Vit D3, Xtandi
J	F	46	24	Breast	n/y	Decadron
K	F	51	41	Breast	y/y	Arimidex, Aromasin, Calcium Citrate, Calcium Gluconate, Docetaxel, Exemestane, Sodium Phosphate, Vit D
L	F	73	24	Lung	y/n	Calcium, Hydroxychloroquine, Vit D
M	F	62	57	Adenocarcinoma	n/n	Hydroxychloroquine, Vit D2
N	F	60	32	Lung	n/n	–
O	M	52	17	Prostate	n/n	Calcium
P	M	72	16	Nasopharyngeal	n/n	Prednisone, Vit D

[a] Only the drug treatments that could affect the bone remodelling are reported.

For each metastatic vertebra the following properties were evaluated:

- Type of metastasis was identified analysing the qCT images of the entire spines: lytic lesions were identified as regions where the bone exhibited focal lower density than the surrounding bone; blastic lesions were identified as regions with higher density than the surrounding bone; mixed lesions as a mix of the lytic and blastic features [33];
- Position of the metastasis within the vertebral body was identified by using virtual partitioning of the vertebra in the higher resolution qCT images [34] [20]. Briefly, each metastatic vertebral body was divided into three longitudinal regions of interest (ROIs): top, middle and bottom, and each ROI was divided in 9 subregions of interest (subROIs) (Fig. 1). The position of the metastasis was indicated by the subROIs involved.
- Size of the metastasis was evaluated with a manual segmentation of each slice of the higher resolution qCT images using a dedicated image processing software package (AMIRA, ThermoFischer) (Fig. 1). The manual procedure was required because it was not possible to automatically segment the lesion [16] as the grey-scale value of the voxels corresponding to metastatic blastic or mixed tissues was similar to the surrounding bone. The protocol developed here was an extension of the procedure used in [35]: for each specimen, each slice of the qCT scans was inspected and the entire vertebral body and the metastasis were separately segmented and their volumes were calculated. The volume of the metastases was expressed as percentage of the volume of the vertebral body.
- The SINS was evaluated by two expert clinicians (GBB, and AG) following the guidelines reported in [2]. Due to the nature of the specimens, the pain cannot be evaluated and only the radiographical parameters were considered. For this reason, the maximum of the SINS scale was reduced from 18 to 15.

2.3. Biomechanical assessment

A novel biomechanical approach based on the combination of mechanical test and DIC strain analysis was used to evaluate the effects of the metastasis on the vertebral mechanical behaviour. An important detail of the experimental design is that each metastatic vertebra was tested together with its adjacent healthy control, to grant a direct paired comparison.

Each specimen was loaded in four different loading configurations: flexion, right and left lateral bending, and pure compression (Fig. 2). A uniaxial testing machine (Instron 8500 controller with Instron 25kN load cell, Instron, UK) was used. To obtain flexion and lateral bending, an eccentric load with respect to the middle intervertebral disc was applied. Flexion was obtained with an anterior eccentricity equal to the 10% of the antero-posterior dimension of the middle intervertebral disc, similar to [36]. The right and left lateral bending were obtained with a, respectively, right and left eccentricity equal to 10% of the right-left dimension of the middle intervertebral disc. In order to avoid any transmission of undesired load components, the top of the spine segment was free to rotate and translate by means of a ball-joint and two low-friction orthogonal linear bearing. Instead, the pure compression was obtained fixing both the top and the bottom of the spine segment to the testing machine and applying a compressive force.

In order to load the different specimens (thoracic or lumbar sections, from donors with different BMI) under comparable conditions, the loading protocol aimed to reach the same strain level in the control vertebral body (measured with Digital Image Correlation, DIC, see below). Each spine segment was loaded until the average minimum principal strain on the most relevant portion of the control vertebra (anterior for flexion and pure compression, lateral for lateral bending) reached approximately −3000 microstrain (range −2500 to −3500 microstrain). This strain magnitude was chosen as a target in order to remain in elastic regime without damaging the bone because it corresponds to the strain levels measured during physiological motor tasks [37]. Ten preconditioning cycles up to half of the target strain value were applied. Then, each specimen was loaded monotonically to reach

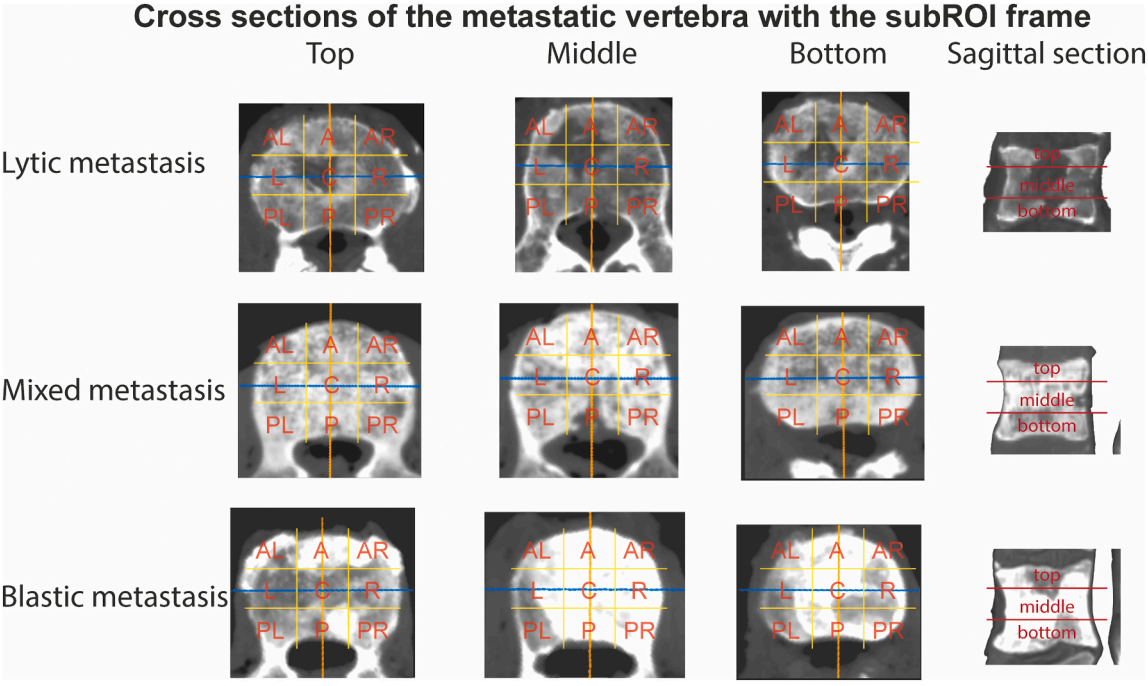

Fig. 1. Definition of the ROI: top, middle and bottom, and of the subROIs: anterior (A), anterior-left (AL), anterior-right (AR), central (C), left (L), right (R), posterior (P), posterior-left (PL) and posterior-right (PR). Examples of typical specimens, for each metastasis type, are reported in order to show the feasibility of manually segmenting the metastases.

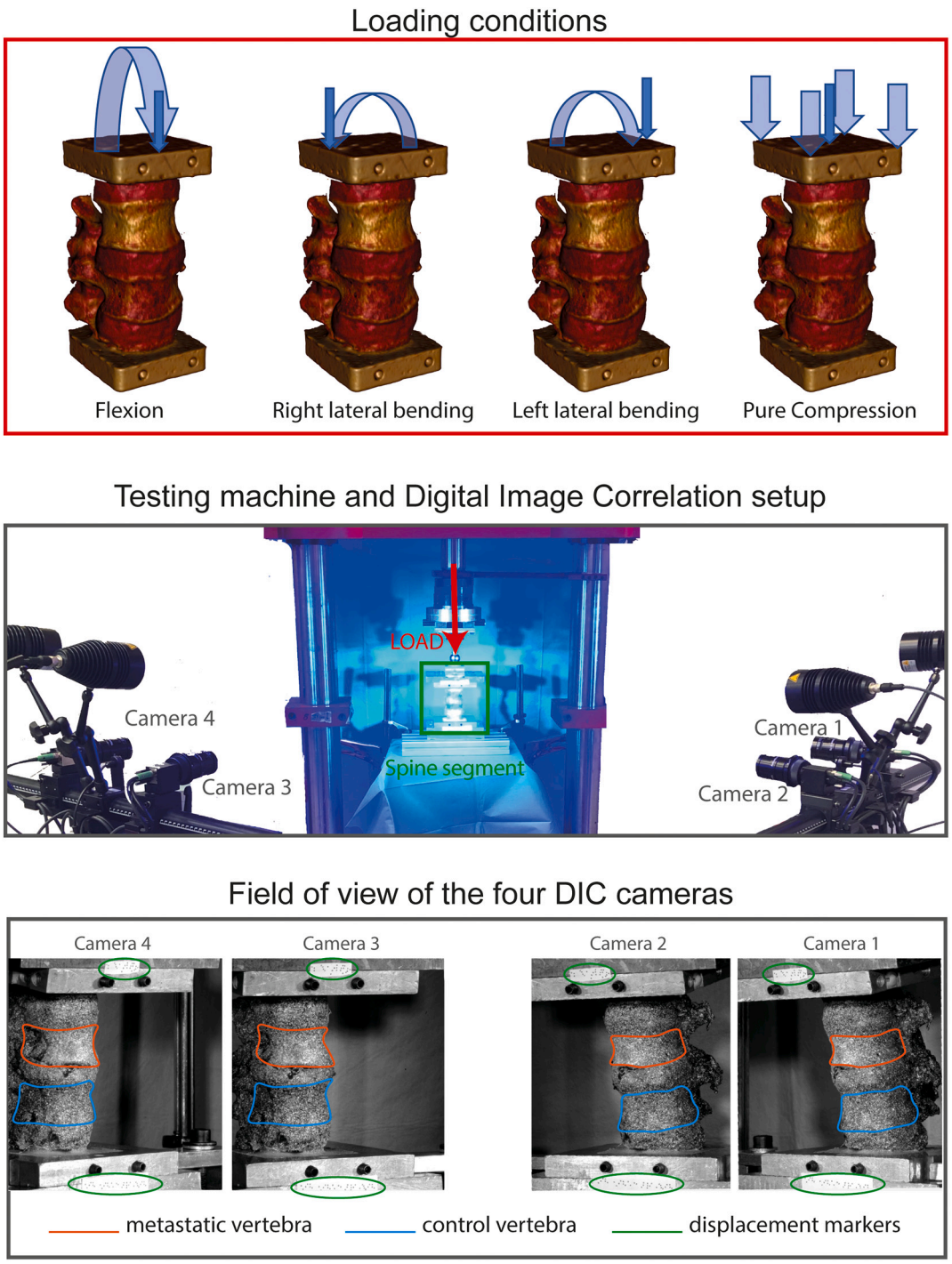

Fig. 2. In the top: the four different loading conditions, the darker arrow indicates the application of the load, the lighter arrow the overall effect. In the middle the mechanical and DIC setup used to evaluate the full-field strain distribution on the spine segment (green box). In the bottom: the field of view acquired by each camera of the DIC system with an indication of the vertebra with metastasis (orange contour), the control vertebra (blue contour) and the markers used to track the displacement of the pots (green ellipse). (For interpretation of the references to colour in this figure legend, the reader is referred to the web version of this article.)

the target strain in 1.0 s.

A state-of-the-art DIC system (Aramis Adjustable 12M, GOM, Braunschweig, Germany) was used to measure the full-field strain distributions [24] on the anterior and lateral surface of the vertebral bodies (Fig. 2, Table 2). Five images of the unloaded specimen were acquired to evaluate the measurement uncertainties [24]. Then, images were acquired at 25 Hz during the three load cycles to measure the deformation.

The maximum (tensile) and minimum (compressive) principal strain and shear strain fields were measured all around the vertebral bodies, as the strain is excellent indicator of how close to failure the bone is [22]. To analyze the metastatic and the control vertebrae in the relevant regions for the different loading conditions, the cortical surface was divided in subROIs (Figs. 1, 3). The mean values of the minimum principal strains were computed in each subROI. The percentage strain difference was computed for each loading condition as the difference between the strain in the middle suROIs of the metastatic vertebra and the strain in the control vertebra, divided by the minimum principal strain evaluated in the middle subROIs of the control vertebra (Fig. 3).

Table 2
Set hardware and software parameters of the DIC.

DIC hardware setup	
Cameras resolution	4 × 12Mpixels (4096 × 3000 pixels)
Camera lenses	4× Titanar B 75, f4.5
Light system	4× LEDs lights with 10° light cone
Measurement volumes	110 × 80 × 80 mm^3 (for smaller specimens)/180 × 130 × 130 mm^3 (for larger specimens)
Pixel size	0.03 mm/0.04 mm
DIC software setup	
Frame rate	25 Hz
Facet size	30 pixels
Grid spacing	10 pixels
Spatial filtering	Median on 5 facets
Temporal filtering	Median on 2 frames
Spackle pattern	White, made with an airbrush-airgun and acrylic water-based paint

The percentage strain difference was used to indicate if and to what extent the metastatic vertebra was more (positive values) or less (negative values) deformed then the control vertebra.

2.4. Statistical analysis

In order to test the hypothesis that the features of the metastases, such as the type, the size of the lesion and its position with respect to the loading conditions, are determinants of the relative deformation of the metastatic vertebra with respect to the control one, the following statistical analyses were performed (Prism 9, GraphPad Software, USA).

To confirm that the metastatic and control vertebrae of each specimen had different behaviours, the respective distributions of minimum principal strains were compared with the Kolmogorov-Smirnov test. To test if differences existed among the minimum principal strains of the different types of vertebrae (control or metastatic), types of metastases, and loading conditions, the Kruskal-Wallis test was performed (data were not normal and homoscedastic, Shapiro-Wilk test and Levene's test).

The percentage strain difference was assumed as a scalar indicator (dependent factor) to summarize the difference of the strain pattern of the metastatic vertebra with respect to the strain pattern of the control vertebra. All the independent parameters (type of metastasis, size of metastasis, SINS, loading condition, if the metastasis was in anterior, in posterior, in right and in left side) were considered for a multivariate analysis in order to evaluate the overall correlation with the percentage strain difference, and which of the parameters had strong agreement. Then intergroup correlations of single independent parameters were performed, as a representation of the different aspects. As we suspected that the percentage strain difference related to the metastasis type or the imposed loading condition (independent factors), Kruskal-Wallis tests with a Dunn's multicomparison analysis were performed (Data were not normal and homoscedastic, Shapiro-Wilk test and Levene's test).

As we found that the percentage strain difference related to the metastasis type, the association between the size of the defect and the percentage strain difference was evaluated with linear correlation analyses, separately for the three types of metastases. To evaluate the correlation between the clinically used score and the biomechanical evidence, a correlation analysis was performed also between the SINS and the percentage strain difference.

The effect of the position of the metastasis with respect to the load was explored only for the metastases located laterally (right or left). Only the lytic metastases were considered, as only for these a strong significant correlation was found in the previous steps. The ipsilateral scenario was defined as the case where the vertebra with a lateral metastasis (e.g. on the right) was loaded towards the same side (e.g. right lateral bending). In the contralateral scenarios the vertebra was loaded in the opposite side of the metastasis (e.g. left bending on a metastasis on the right side). Cases with only anterior, central, posterior

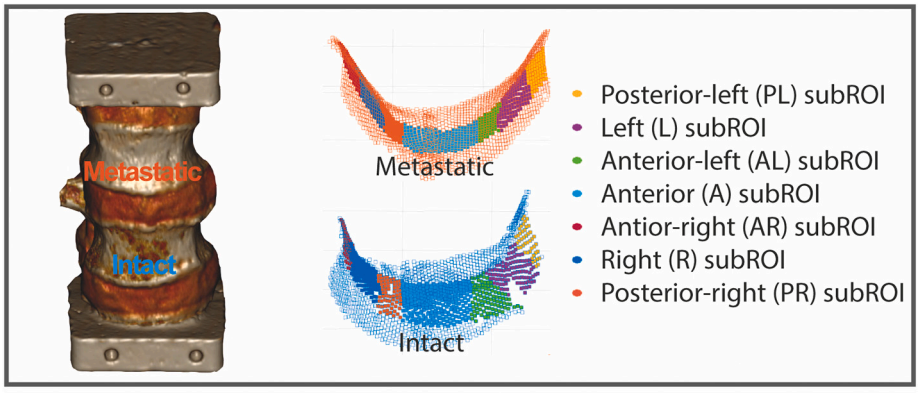

$$\text{Strain Difference (\%)} = \frac{\overline{\varepsilon}\ (\text{metastatic subROIs}) - \overline{\varepsilon}\ (\text{control subROIs})}{\overline{\varepsilon}\ (\text{control subROIs})} \times 100$$

Loading conditions	subROIs for Relative Strain Variation
Flexion	AL, A, AR
Right bending	AR, R, PR
Left bending	AL, L, PL
Pure Compression	all

Fig. 3. On the top: the reconstructed 3D surfaces of a specimens from CT scan and from DIC data of the metastatic (orange) and control (blue) vertebrae, with a colour legend definition of the subROIs on the vertebral body used for the strain analysis. On the bottom: the percentage strain difference was evaluated considering the minimum principal strains (ε) on specific subROIs for each loading conditions, as reported in the table. (For interpretation of the references to colour in this figure legend, the reader is referred to the web version of this article.)

metastasis or spread in the entire vertebra, were excluded, leaving a total of 13 specimens for this analysis. Shapiro-Wilk test confirmed that data were not normally distributed. The Wilcoxon matched-pairs signed rank test was used to test the significance of the difference of the percentage strain difference between ipsilateral and contralateral scenarios.

Once the position of the lytic lesion with respect to the loading direction was taken into account, the agreement between the size of the lytic metastasis and the percentage strain difference, separately for the ipsilateral and contralateral scenarios, was analysed with a linear correlation analysis. Linear correlation analyses were performed also between the SINS and the percentage strain difference, separately, for the ipsilateral and contralateral scenarios.

Finally, a correlation analysis was performed between the SINS and the size of the metastasis.

For every test, the level of significance was set to 0.05. The Pearson's correlation coefficient (r) and the coefficient of determination (r^2) were reported to indicate the level of agreement of the linear correlations.

3. Results

The sample included 18 vertebrae with lytic lesion from nine donors, eleven vertebrae with mixed lesion from seven donors and six vertebrae with blastic lesions from three donors. The metastases were spread from eight different types of primary tumours. All vertebrae of the same donor showed the same type of metastasis, except for donors 6 and 10 (Table 3).

The size of the lytic metastases ranged from 0.3 cm^3 to 10.1 cm^3, the blastic from 9.3 cm^3 to 24 cm^3, the mixed metastases from 1.4 cm^3 to 15.2 cm^3 (Table 3). There was no clear prevalence of a position inside the vertebral body with respect to another considering the different metastasis type.

The maximum and minimum principal strains and the shear strain maps were evaluated for all specimens in the metastatic and control vertebrae, in all loading conditions (see Fig. 4, Supplementary Materials 1 and 2), except for ID1, ID19 and ID24 in flexion, ID19 and ID31 in pure compression, where the DIC analysis was compromised by blood and

Table 3
List of the specimens (ID in first column from 1 to 35) obtained from the 16 donors (labelled as A, B, … P) who suffered from different primary tumours (summary from Table 1). For each specimen the position in the spine of the metastatic vertebra is indicated, as well as the extension of the test specimen (spine segment). The clinical evaluations are reported in terms of metastasis type, size, position and SINS. The last columns summarize the experimental findings in terms of percentage strain difference for the different loading conditions.

ID	(Donor and primary tumour)	Metastatic vertebra	Spine segment	Metastasis type	Lesion size (VB% (cm^3))	Position	SINS[a]	Percentage strain difference			
								Flexion	Right lateral bending	Left lateral bending	Pure compression
1	A, adrenal	T4	T2-T5	Lytic	14 (3.0)	C, L, P, PL	4	NA	−28%	+70%	+5%
2		T6	T5-T8	Lytic	16 (4.3)	C, P, R	3	+7%	−30%	+283%	+43%
3		L2	T12-L3	Lytic	11 (6.2)	A, AL, C, L	6	−23%	−51%	+149%	+16%
4	B, lung	T11	T9-L1	Blastic	14 (7.2)	AL, C, P, PR	6	+19%	+138%	+20%	+27%
5		T12	T9-L1	Blastic	17 (9.5)	ALL	6	0%	−8%	+41%	−32%
6		L4	L2-S	Blastic	14 (9.4)	AL, L, PL, PR	6	+31%	+18%	−25%	+7%
7		L5	L2-S	Blastic	17 (9.5)	all	6	−23%	+6%	+101%	+158%
8	C, uterine	T10	T9-L1	Lytic	1 (0.3)	C	3	+42%	+178%	−5%	−56%
9		T11	T9-L1	Lytic	2 (0.4)	A	5	+90%	+380%	+104%	+163%
10	D, lung	L2	L1-L4	Lytic	36 (10.1)	R, C, PR, P	5	+34%	+1280%	−2%	+401%
11	E, bladder	T12	T10-L1	Mixed	4 (1.4)	AR, A, AL	8	+58%	0%	+8%	+84%
12	F, breast	T6	T5-T8	Lytic	5 (0.6)	A, L, PL	3	−37%	−53%	+91%	−7%
13		T11	T9-T12	Mixed	12 (2.2)	PR, R	4	+45%	+298%	−12%	+51%
14		L2	L1-L5	Lytic	11 (2.8)	A, R, C, L, PL	4	+149%	+2%	+217%	+72%
15		L4	L1-L5	Lytic	20 (5.2)	A, C	4	+77%	−33%	+26%	+41%
16	G, breast	T4	T3-T6	Lytic	47 (5.4)	R, L	11	+1374%	+138%	+1127%	+1135%
17		T8	T6-T9	Lytic	12 (2.0)	AR, A, AL, L, P, PL	5	+54%	+158%	+150%	+126%
18		T11	T9-T12	Lytic	20 (5.0)	A, AL, L, P, PL	7	−41%	+53%	+138%	+66%
19		L2	T12-L3	Lytic	14 (3.5)	all	10	NA	−37%	−61%	NA
20	H, prostate	L4	L2-L5	Blastic	25 (9.3)	A, AL, P, PL, C	5	+93%	−6%	−61%	+2%
21	I, prostate	L2	T12-L3	Blastic	59 (24.0)	A, C, P, PL	5	−51%	−66%	−8%	−18%
22		L5	L3-S	Mixed	28 (15.2)	all	8	−65%	−85%	+34%	−34%
23	J, breast	T8	T7-T10	Mixed	36 (5.5)	all	6	−54%	−30%	+17%	+81%
24		T11	T10-L1	Lytic	30 (8.4)	A, AR, R	8	NA	+570%	+104%	+541%
25	K, breast	T6	T5-T8	Mixed	31 (4.3)	A, R, C, L, P	7	+214%	+96%	+66%	+35%
26		T12	T11-L2	Mixed	19 (5.3)	all	7	−13%	−44%	−48%	−57%
27		L5	L3-S	Mixed	20 (8.6)	A, L, C	7	−55%	−68%	+150%	−35%
28	L, lung	T7	T6-T9	Mixed	33 (5.3)	R, C, PR, P	6	+19%	+44%	+8%	+1%
29		T12	T10-L1	Mixed	12 (3.6)	AR, A, AL, R	4	−67%	−31%	+21%	−12%
30		L2	L1-L4	Mixed	27 (9.9)	all	4	+177%	+131%	+56%	+163%
31	M, adenocarcinoma	T5	T4-T7	Lytic	6 (0.8)	R	3	+17%	+118%	−7%	NA
32	N, lung	L2	T12-L4	Lytic	10 (4.5)	A, R, C	8	+46%	−53%	+564%	+31%
33	O, prostate	T8	T6-T9	Mixed	47 (10.0)	all	5	−36%	−86%	−79%	−34%
34	P, nasopharyngeal	T5	T4-T8	Lytic	7 (0.6)	C, L, P, PL	4	−43%	−8%	+16%	−38%
35		T6	T4-T8	Lytic	10 (1.0)	C, L, PL	4	+13%	+2%	−7%	−59%

[a] SINS based only on the radiographical parameters. NA represents not available results due to poor DIC correlation.

marrow leakage. The measurement uncertainties were approximately 30 microstrains for the systematic error and 100 microstrains for the random error, in line with previous DIC analyses [9,27].

The strain distributions in the metastatic and control vertebrae of the same specimen under the same load were statistically different (Kolmogorov-Smirnov test, $p < 0.05$). The minimum principal strain (Fig. 5) had different distributions for each type of metastasis (Kruskal-Wallis, $p = 0.04$) and the different loading conditions (Kruskal-Wallis, p 0.003).

In case of lytic metastases, the full-field maps showed larger strains on the metastatic vertebrae, in correspondence of the lesion. Conversely, in case of blastic metastasis larger strains were found on the control vertebrae. Mixed metastases did not show a clear systematic behaviour: areas with increased and with decreased strain magnitude were observed on the same vertebra according to the nature of the underlying coexisting metastatic tissues (blastic or lytic) (Fig. 4).

The percentage strain difference (Table 3, and Supplementary material 2) summarizes the strain differences between the metastatic and control vertebra of the same spine segment. The multivariate analysis showed that the explored parameters could partially explain the variability of the percentage strain difference, with high statistical significance ($r = 0.62$, $r^2 = 0.38$, $p < 0.0001$). In particular, the loading conditions and the position of the metastasis in the left side showed non-significant correlation ($p = 0.98$ and $p = 0.85$, respectively). The other parameters (type of metastasis, size of metastasis, SINS, if the metastasis was in anterior, in posterior and in right side) instead were all significant ($p < 0.05$). The percentage strain difference (Table 3) was influenced by the type of metastasis (Kruskal-Wallis test, $p = 0.0004$) but not by the loading conditions ($p = 0.48$). In particular, the percentage strain difference was significantly different between the mixed and lytic metastases (p = 0.0004). Conversely, differences were not significant between blastic and mixed ($p > 0.98$), and between lytic and blastic ($p = 0.11$) metastases.

No statistically significant agreement was found between the percentage strain difference and the size of the metastasis ($p = 0.072$, Fig. 6a), when all the types of metastases were pooled. When the specimens were split by metastasis type, a positive correlation between the percentage strain difference and the size of the lytic metastasis ($r = 0.64$, $r^2 = 0.41$, $p < 0.0001$, Fig. 6b) was observed. This indicates that the larger the lytic lesions, the higher the strain on the metastatic vertebra. Weak but significant, negative correlations were found between the percentage strain difference and the size of blastic lesion ($r = -0.43$, $r^2 = 0.18$, $p = 0.037$) as well as between the percentage strain difference and the size of mixed lesion ($r = -0.30$, $r^2 = 0.09$, $p = 0.045$). Once the position of the lytic lesion with respect to the loading direction was taken into account (ipsilateral and contralateral scenarios), the respective percentage strain differences were grouped separately. The Wilcoxon matched-pairs signed rank test revealed no statistical difference ($p = 0.16$) between ipsilateral and contralateral scenarios. Finally, in case of lytic metastases in the ipsilateral scenarios, the lesion size showed an excellent significant, positive correlation with the percentage strain difference ($r = 0.85$, $r^2 = 0.72$, $p = 0.0002$; Fig. 6c), while no correlation was found for the contralateral scenarios ($p = 0.97$).

The SINS computed as the sum of the objective parameters ranged from 3 to 11 (Table 3). A significant but weak correlation was found between SINS and the percentage strain difference ($r = 0.30$, $r^2 = 0.09$, $p = 0.0003$, Fig. 6b). The agreement was strengthened, if only the lytic metastases were considered ($r = 0.50$, $r^2 = 0.25$, $p < 0.0001$, Fig. 6b). In case of other metastasis types, the agreement was not statistically

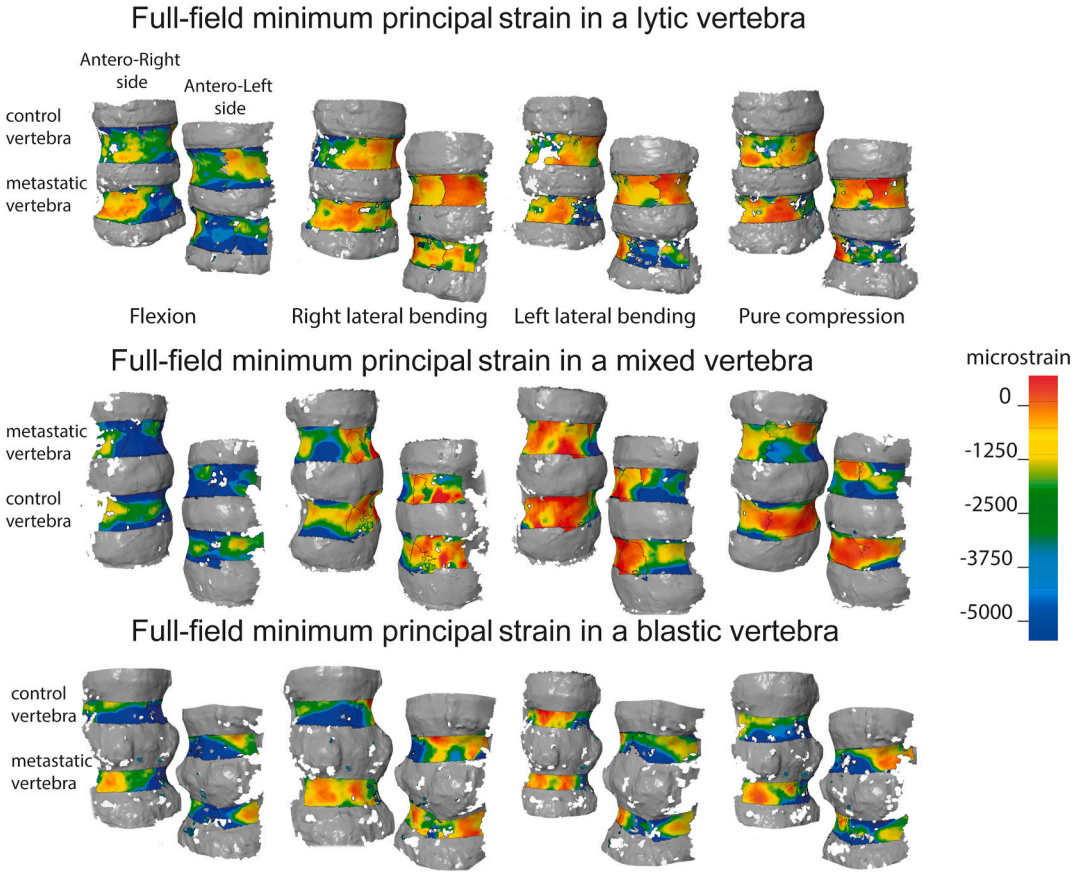

Fig. 4. Full-field minimum principal strains evaluated for each loading conditions (from left: flexion, right lateral bending, left lateral bending pure compression, see Fig. 2) in segments with a lytic, mixed and blastic metastasis. For each specimen, views both from the anterior-right and anterior-left sides are reported. The specimens reported here are the same showed in Fig. 1.

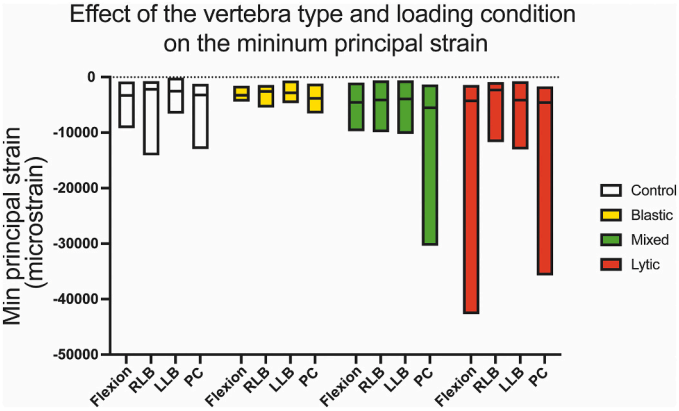

Fig. 5. Box plot of the min principal strains (top) evaluated for the specimens grouped as control and for type of metastasis in each loading conditions (flexion, RLB: right lateral bending, LLB: left lateral bending, PC: pure compression). The box plot shows for each group the median and the full range.

significant (mixed $p = 0.52$, blastic $p = 0.07$). No significant agreement was found between SINS and the percentage strain difference, when the position of the metastasis, in terms of ipsilateral (p = 0.52) and contralateral ($p = 0.12$) scenarios, was taken into account (Fig. 6c).

Finally, no statistical correlation existed between the SINS and the size of the metastasis ($p = 0.061$).

4. Discussion

In this study, a sample of spine segments with real metastases, spread from different primary tumours, was tested in different loading conditions to evaluate if the type, the size and position of the metastasis are determinants of the deformation of the metastatic vertebra.

This work showed that the size and position of the lytic lesions explain the critical deformation of the vertebrae, while blastic and mixed lesions do not induce a univocal trend in the vertebrae and a more detailed local analysis would be necessary to clearly explain the different behaviours.

In general, the metastasis type, which is associated with the mineral content [16], the mineral distribution and the crystal size [3] of the bone, determines the behaviour of the vertebra.

The vertebrae with lytic metastasis showed significant correlations between the properties of the lesions and the relative deformation of the vertebrae. High deformation was found in the vertebrae where the lesions were larger than the 30% of the vertebral body and close to the cortical shell [38]. The size of the lytic metastasis was confirmed by the biomechanical outcomes as a clear indicator of the spine instability [9,11,35]. The percentage strain difference associated with the position of the lytic metastasis (ipsilateral and contralateral scenarios) did not show differences. It means that considering only the size or only the position of the metastasis provides a partial explanation of the phenomena. A conjoint evaluation of the lytic dimension and the lytic position with respect to the loading direction, instead, nearly doubled the explanatory power of the mechanical indicator ($r^2 = 0.72$). This reveals i) the importance of a general evaluation of the metastasis intrinsic parameters, ii) the importance of the internal structure [13,15,39] and iii) the integrity of the cortical shell [40,41]. Moreover, the spine instability as a consequence of the lytic lesion lead to hypothesize the lack of reorganization and re-optimization [42,43] of the surrounding tissues.

The vertebra with blastic metastases showed, instead, a completely different behaviour [44]. As reported in other studies, the strength of vertebrae with blastic lesion is higher than the vertebrae with lytic lesions [16,45]. However, the control vertebrae were subjected to localized strain concentrations in the location corresponding to the adjacent blastic metastasis, which seemed to act as stress concentrators. This only partially reflects the fragility of the blastic vertebra, sometimes reported in the clinical practice [46], especially in cases of metastases derived from prostate tumours. It is interesting to note that the percentage strain difference of the metastatic vertebrae from the patients treated with corticosteroids were systematically lower (i.e. less critical) than those from patients without any treatment (Mann-Whitney test, p-value = 0.028) [47]. However, considering the small number (three donors, providing 16 percentage strain difference values evaluated on vertebrae from non-treated subjects and 8 from subjects treated with corticosteroids), additional studies must be performed to generalize this preliminary observation.

The mixed metastasis showed patches with both strain concentration and reduction, reflecting the local mix of blastic and lytic tissue, that did not allow the recognition of an overall systematic behaviour. This result confirmed the difficulty of defining a clear guideline for identifying the mixed metastasis at risk of fracture.

The SINS is the current clinical tool to define the spine stability in case of metastatic vertebrae [2]. The SINS evaluated for the same vertebrae had only weak agreement with the mechanical properties [48]. Moreover, the SINS did not correlate with the size of the metastasis. The higher agreement obtained between metastatic features and percentage strain difference means that type, size and position of the metastasis strongly affect the spine stability, increasing the explanatory power compared to the SINS alone. The uncertainty in giving a surgical indication in cases of doubtful instability/fracture risk (SINS 7–12) could be partially improved by the findings produced by this experiment, paving the way to a more detailed image evaluation, reflecting the mechanical evidence.

Different findings were found in the literature to explain the weakness of the metastatic vertebrae, with diverging results about the relevance of the metastasis size and position. For example, the lesion size was considered fundamental in triggering the vertebral fracture in several studies [9,13,15]. By contrast, in other studies the lesion size was a secondary information [10,12]. The position of the lesion was frequently considered having a low relevance [10,12,13,15]. However, in those studies just few loading scenarios were applied to the spines to evaluate the effect of the position of the lesions. In this work an unprecedented series, both in terms of specimens and loading conditions, was tested, for a total of 348 tests. The measurement of the full-field strain distributions allowed to overcomes the limitations of considering only overall apparent global properties (e.g. overall stiffness or failure load) or point-wise strain measurements [8,10,11]. In fact, while the evaluation of the strength would have provided an indicator of the overall failure behaviour of the vertebra in a single loading condition, a strength value to be used as a reference to characterize the metastatic vertebrae was not available in the literature. This would have required a much larger sample size and would not have explained why the metastatic vertebra fails. Conversely, measuring the full-field distribution of

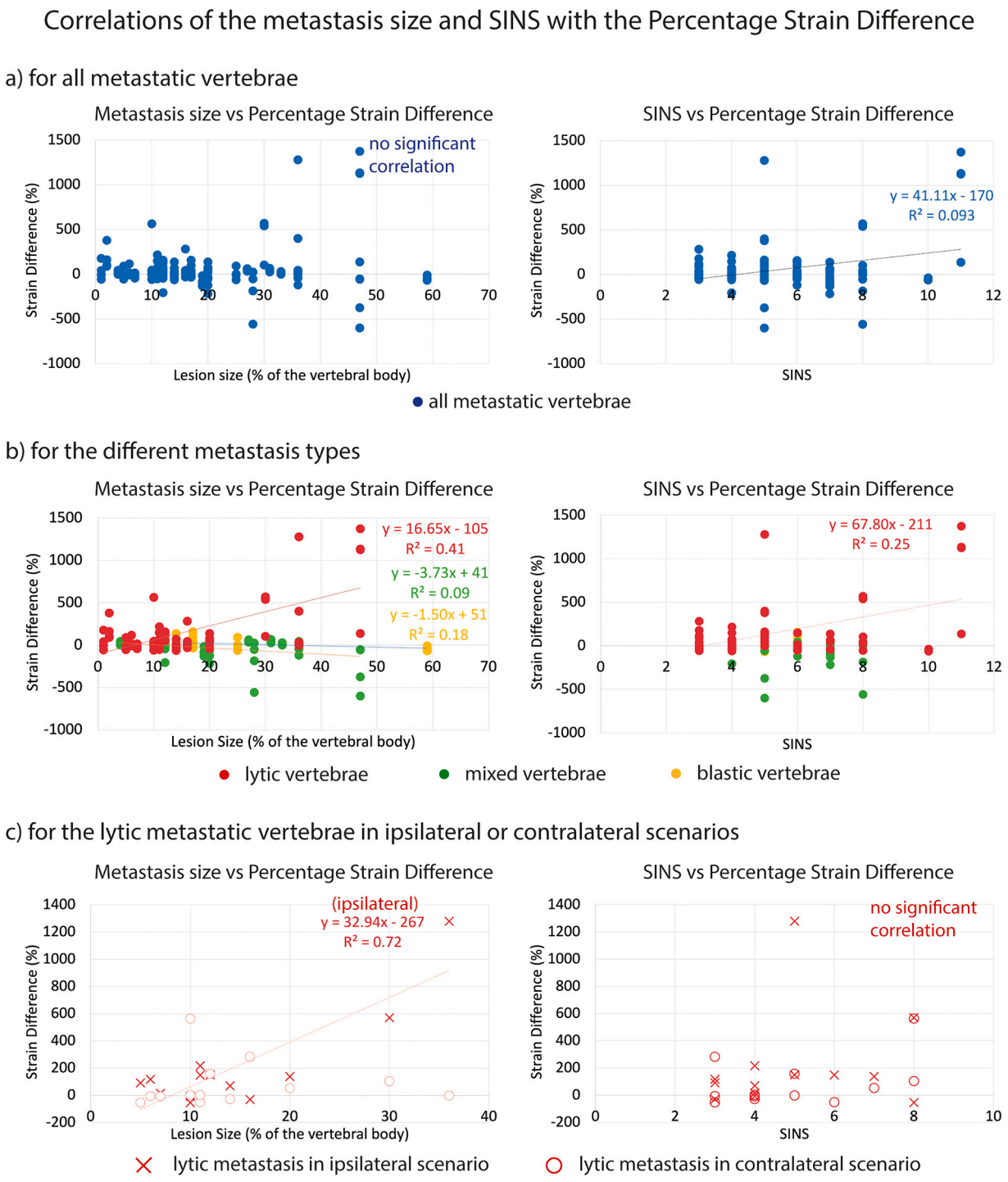

Fig. 6. a) Scatter plots of the percentage strain difference (dependent factor) with respect to the metastasis size (independent factor) on the left and SINS (independent factor) on the right. a) The entire batch of metastatic vertebrae was considered without any additional distinction; b) the metastatic vertebrae were grouped by metastasis type, considering all the loading conditions; c) only the lytic metastatic vertebrae grouped in the ipsilateral and contralateral scenarios.

strains can help elucidate the failure mechanisms and build more reliable predictors of the risk of fracture. Moreover, using the strain [22] and the percentage strain difference as a surrogate of the mechanical competence, enabled a clearer analysis of the local effects of the lesions.

Testing the spine in different loading conditions, enabled the identification of the differences in terms of deformation of the same vertebra with asymmetric lesions, and focus on the relevance of the metastatic position.

The first limitation related to the strain measurements only on the surface of the vertebral body. A comprehensive characterization of the metastatic vertebrae would benefit from measurements of the strain pattern also within the bone. Nevertheless, the role of the cortical shell in the load sharing is maximum at the midsection [40], where the analysis was carried out. Additional Digital Volume Correlation (DVC) analysis [49] could be performed to measure the strain inside the bone and also explore possible load induced canal narrowing.

The type of metastasis was evaluated by two expert spinal oncological surgeons from qCT images, as in the clinical practice, and confirmed by the donors' medical history. This left a minimal uncertainty about the metastasis classification that only the histological analysis would solve

[50]. In the clinical practice, bone scintigraphy and positron emission tomography could further reduce the uncertainties in the metastatic identification evaluating the metabolic activity. However, those techniques are not applicable in vitro.

The qCT images were also used to evaluate the size of the lesions. In view of possible future application of these findings, we chose to use the imaging technique with the best possible resolution available in clinical practice (in plane voxel size of 0.25–0.45 mm, which is sub-optimal for measuring the smallest metastatic lesions) and that enables best to identify the differences in bone density. In fact, the developed method for the evaluation of the metastatic size could be applied in the clinical practice with a minimal effort.

To have a better spatial description, the metastatic position was identified using a classification different by the ones used in the surgical practice, e.g. WBB surgery staging system [51] or the Enneking staging system [52]. The current one allowed a clearer identification of the mechanical effects in the different loading conditions concerning only the vertebral body.

The percentage strain difference was defined in order to obtain a clear and easy-to-use scalar indicator of the differences between a metastatic vertebra and a control vertebra, instead of using two tensor quantities (strains). The percentage strain difference enabled a direct comparison among the different groups, and quantifies to what extent the metastatic vertebra is more (or less) deformed than the adjacent control vertebra. Indeed, there are mechanistic reasons to explain that adjacent vertebrae underwent similar loads during the donors' motor tasks [53], and similar strength (thus, strain distribution) could be expected when both are healthy [24].

The loading conditions aimed to mimic basic physiological loads. This solution could seem far from the daily physiological loads but allowed to clearly separate and highlight the effect of the metastasis position for the different loading directions. To enable subsequent additional investigations, fracture was not reached. While this does not invalidate the identification of the biomechanical behaviour of the metastatic vertebrae [9,31], the definitions of a critical size and location of the lesions that trigger the vertebral failure, was not possible.

Finally, the SINS was only evaluated considering the objective radiographic parameters without considering the pain, that has a relevant weight in the decision making. For this reason, an objective quantification that allowed looking at the trend and the agreements, and not the threshold associated to the different outcomes, was preferred.

In this work we tested spine segments with a metastatic and a control (free of metastasis) vertebra to minimize the uncertainty caused by the variability of the single metastatic vertebrae and the different donors. The percentage strain difference compares the strain magnitudes of two adjacent vertebrae subjected to the same load but with intrinsic different characteristics (control vs metastasis). The use of a large field of view DIC cameras enabled to cover the entire surface, from one peduncle to the other, allowing to take into account the entire field of deformations also in apparently not relevant regions. Unprecedented evidence about the biomechanical importance of the size and position of the metastasis in the spine stability is presented. However, follow up studies are mandatory to better identify the warning size thresholds and defining specific motor tasks that mostly stress the spine with metastases in a specific location.

In conclusion, our results suggest considering the location and size of the lytic component of skeletal metastasis as an important driver of biomechanical spinal instability and highlight its potential in clinical practice for improving our current scoring system.

Supplementary data to this article can be found online at https://doi.org/10.1016/j.bone.2021.116028.

CRediT authorship contribution statement

Marco Palanca: Conceptualization, Methodology, Investigation, Data curation, Writing – original draft, Project administration, Funding acquisition. **Giovanni Barbanti-Bròdano:** Conceptualization, Investigation, Writing – review & editing, Supervision. **Daniele Marras:** Investigation, Data curation, Writing – review & editing. **Mara Marciante:** Investigation, Writing – review & editing. **Michele Serra:** Investigation, Writing – review & editing. **Alessandro Gasbarrini:** Investigation, Writing – review & editing. **Enrico Dall'Ara:** Conceptualization, Funding acquisition, Resources, Writing – review & editing. **Luca Cristofolini:** Conceptualization, Methodology, Resources, Writing – review & editing, Project administration, Supervision.

Declaration of competing interest

The authors have no conflict of interest to declare.

Acknowledgements

The authors gratefully acknowledge Prof Marco Viceconti for sharing his prospective view and the stimulating discussions, Prof Cinzia Viroli for the help in the statistical analysis, MD Elena Pelizzaro for evaluating the clinical history of the donors, Ms. Pierangela Moro for the help during the qCT scans and Ms. Giulia Cavazzoni for proof-reading the manuscript.

The study was partially funded by the AOSpine Discovery and Innovation Awards (AOSDIA 2019_063_TUM_Palanca), Marie Skłodowska-Curie Individual Fellowship (MetaSpine, MSCA-IF-EF-ST, 832430/2018) and by the Engineering and Physical Sciences Research Council (EPSRC) Frontier Multisim Grant (EP/K03877X/1 and EP/S032940/1).

MP acknowledges Christine Sephton for encouraging us to perform this study.

References

[1] I. Laufer, D.G. Rubin, E. Lis, B.W. Cox, M.D. Stubblefield, Y. Yamada, M.H. Bilsky, The NOMS framework: approach to the treatment of spinal metastatic tumors, Oncologist 18 (2013) 744–751, https://doi.org/10.1634/theoncologist.2012-0293.

[2] C.G. Fisher, C.P. DiPaola, T.C. Ryken, M.H. Bilsky, C.I. Shaffrey, S.H. Berven, J.S. Harrop, M.G. Fehlings, S. Boriani, D. Chou, M.H. Schmidt, D.W. Polly, R. Biagini, S. Burch, M.B. Dekutoski, A. Ganju, P.C. Gerszten, Z.L. Gokaslan, M.W. Groff, N.J. Liebsch, E. Mendel, S.H. Okuno, S. Patel, L.D. Rhines, P.S. Rose, D.M. Sciubba, N. Sundaresan, K. Tomita, P.P. Varga, L.R. Vialle, F.D. Vrionis, Y. Yamada, D.R. Fourney, A novel classification system for spinal instability in neoplastic disease: an evidence-based approach and expert consensus from the spine oncology study group, Spine. 35 (2010) E1221–E1229. doi:https://doi.org/10.1097/BRS.0b013e3181e16ae2.

[3] M. Burke, A. Atkins, A. Kiss, M. Akens, A. Yee, C. Whyne, The impact of metastasis on the mineral phase of vertebral bone tissue, J. Mech. Behav. Biomed. Mater. 69 (2017) 75–84, https://doi.org/10.1016/j.jmbbm.2016.12.017.

[4] D.R. Fourney, E.M. Frangou, T.C. Ryken, C.P. DiPaola, C.I. Shaffrey, S.H. Berven, M.H. Bilsky, J.S. Harrop, M.G. Fehlings, S. Boriani, D. Chou, M.H. Schmidt, D.W. Polly, R. Biagini, S. Burch, M.B. Dekutoski, A. Ganju, P.C. Gerszten, Z.L. Gokaslan, M.W. Groff, N.J. Liebsch, E. Mendel, S.H. Okuno, S. Patel, L.D. Rhines, P.S. Rose, D. M. Sciubba, N. Sundaresan, K. Tomita, P.P. Varga, L.R. Vialle, F.D. Vrionis, Y. Yamada, C.G. Fisher, Spinal instability neoplastic score: an analysis of reliability and validity from the spine oncology study group, JCO. 29 (2011) 3072–3077. doi: https://doi.org/10.1200/JCO.2010.34.3897.

[5] S. Fox, M. Spiess, L. Hnenny, Daryl.R. Fourney, Spinal instability neoplastic score (SINS): reliability among spine fellows and resident physicians in orthopedic surgery and neurosurgery, Glob. Spine J. 7 (2017) 744–748, https://doi.org/10.1177/2192568217697691.

[6] A.L. Versteeg, J.M. Velden, H.M. Verkooijen, M. Vulpen, F.C. Oner, C.G. Fisher, J. Verlaan, The effect of introducing the spinal instability neoplastic score in routine clinical practice for patients with spinal metastases, Oncologist 21 (2016) 95–101, https://doi.org/10.1634/theoncologist.2015-0266.

[7] R.N. Alkalay, Effet of the metastatic defect on the structural responde and failure process of human vertebrae: an experimental study, Clin. Biomech. 30 (2015) 121–128.

[8] R.N. Alkalay, T.P. Harrigan, Mechanical assessment of the effects of metastatic lytic defect on the structural response of human thoracolumbar spine: effect of critical lytic defect, J. Orthop. Res. 34 (2016) 1808–1819, https://doi.org/10.1002/jor.23154.

[9] M. Palanca, G. Barbanti-Bròdano, L. Cristofolini, The size of simulated lytic metastases affects the strain distribution on the anterior surface of the vertebra, J. Biomech. Eng. 140 (2018) 111005, https://doi.org/10.1115/1.4040587.

[10] M.J. Silva, J.A. Hipp, D.P. McGowan, T. Takeuchi, W.C. Hayes, Strength reductions of thoracic vertebrae in the presence of transcortical osseous defects: effects of defect location, pedicle disruption, and defect size, Eur. Spine J. 2 (1993) 118–125, https://doi.org/10.1007/BF00301407.

[11] C.M. Whyne, S.S. Hu, J.C. Lotz, Burst fracture in the Metastatically involved spine: development, validation, and parametric analysis of a three-dimensional poroelastic finite-element model, Spine. 28 (2003) 652–660, https://doi.org/10.1097/01.BRS.0000051910.97211.BA.

[12] H.J. Windhagen, J.A. Hipp, M.J. Silva, Lipson, S J, W.C. Hayes, Predicting failure of thhoracic vertebrae with simulated and actual metastatic defects, Clin. Orthop. Relat. Res. 344 (1997) 313–319.

[13] M.C. Costa, L.B.B. Campello, M. Ryan, J. Rochester, M. Viceconti, E. Dall'Ara, Effect of size and location of simulated lytic lesions on the structural properties of human vertebral bodies, a micro-finite element study, Bone Rep. 12 (2020) 100257, https://doi.org/10.1016/j.bonr.2020.100257.

[14] M.C. Costa, P. Eltes, A. Lazary, P.P. Varga, M. Viceconti, E. Dall'Ara, Biomechanical assessment of vertebrae with lytic metastases with subject-specific finite element models, J. Mech. Behav. Biomed. Mater. 98 (2019) 268–290, https://doi.org/10.1016/j.jmbbm.2019.06.027.

[15] F. Galbusera, Z. Qian, G. Casaroli, T. Bassani, F. Costa, B. Schlager, H.-J. Wilke, The role of the size and location of the tumors and of the vertebral anatomy in determining the structural stability of the metastatically involved spine: a finite element study, Transl. Oncol. 11 (2018) 639–646, https://doi.org/10.1016/j.tranon.2018.03.002.

[16] M.A. Stadelmann, D.E. Schenk, G. Maquer, C. Lenherr, F.M. Buck, D.D. Bosshardt, S. Hoppe, N. Theumann, R.N. Alkalay, P.K. Zysset, Conventional finite element models estimate the strength of metastatic human vertebrae despite alterations of the bone's tissue and structure, Bone 141 (2020) 115598, https://doi.org/10.1016/j.bone.2020.115598.

[17] C.E. Tschirhart, J.A. Finkelstein, C.M. Whyne, Biomechanics of vertebral level, geometry, and transcortical tumors in the metastatic spine, J. Biomech. 40 (2007) 46–54, https://doi.org/10.1016/j.jbiomech.2005.11.014.

[18] C.E. Tschirhart, A. Nagpurkar, C.M. Whyne, Effects of tumor location, shape and surface serration on burst fracture risk in the metastatic spine, J. Biomech. 37 (2004) 653–660, https://doi.org/10.1016/j.jbiomech.2003.09.027.

[19] C.M. Whyne, S.S. Hu, Parametric finite element analysis of vertebral bodies affected by tumors, J. Biomech. 34 (2001) 1317–1324.

[20] M. Palanca, G. De Donno, E. Dall'Ara, A novel approach to evaluate the effects of artificial bone focal lesion on the three-dimensional strain distributions within the vertebral body, PLoS ONE. under review (n.d.).

[21] P. Sutcliffe, M. Connock, D. Shyangdan, R. Court, N.-B. Kandala, A. Clarke, A systematic review of evidence on malignant spinal metastases: natural history and technologies for identifying patients at high risk of vertebral fracture and spinal cord compression, Health Technol. Assess. 17 (2013). doi:https://doi.org/10.3310/hta17420.

[22] U. Wolfram, J. Schwiedrzik, Post-yield and failure properties of cortical bone, Bonekey Rep. 5 (2016). doi:https://doi.org/10.1038/bonekey.2016.60.

[23] M. Palanca, G. Tozzi, L. Cristofolini, The use of digital image correlation in the biomechanical area: a review, Int. Biomech. 3 (2016) 1–21, https://doi.org/10.1080/23335432.2015.1117395.

[24] M. Palanca, M. Marco, M.L. Ruspi, L. Cristofolini, Full-field strain distribution in multi-vertebra spine segments: an in vitro application of digital image correlation, Med. Eng. Phys. 52 (2018) 76–83, https://doi.org/10.1016/j.medengphy.2017.11.003.

[25] M. Palanca, T.M. Brugo, L. Cristofolini, Use of digital image correlation to investigate the biomechanics of the vertebra, J. Mech. Med. Biol. 15 (2015) 1540004, https://doi.org/10.1142/S0219519415400047.

[26] H. Gustafson, G. Siegmund, P. Cripton, Comparison of strain rosettes and digital image correlation for measuring vertebral body strain, J. Biomech. Eng. 138 (2016), 054501, https://doi.org/10.1115/1.4032799.

[27] M. Palanca, M.L. Ruspi, L. Cristofolini, C. Liebsch, T. Villa, M. Brayda-Bruno, F. Galbusera, H.-J. Wilke, L. La Barbera, The strain distribution in the lumbar anterior longitudinal ligament is affected by the loading condition and bony features: an in vitro full-field analysis, PLoS ONE 15 (2020), e0227210, https://doi.org/10.1371/journal.pone.0227210.

[28] Ruspi, Palanca, Cristofolini, Liebsch, Villa, Brayda-Bruno, Galbusera, Wilke, La Barbera, Digital image correlation (DIC) assessment of the non-linear response of the anterior longitudinal ligament of the spine during flexion and extension, Materials 13 (2020) 384, https://doi.org/10.3390/ma13020384.

[29] T.P. Holsgrove, D. Cazzola, E. Preatoni, G. Trewartha, A.W. Miles, H.S. Gill, S. Gheduzzi, An investigation into axial impacts of the cervical spine using digital image correlation, Spine J. 15 (2015) 1856–1863, https://doi.org/10.1016/j.spinee.2015.04.005.

[30] H.M. Gustafson, A.D. Melnyk, G.P. Siegmund, P.A. Cripton, Damage identification on vertebral bodies during compressive loading using digital image correlation:, Spine. 42 (2017) E1289–E1296. doi:https://doi.org/10.1097/BRS.0000000000002156.

[31] M. Palanca, L. Cristofolini, A. Gasbarrini, G. Tedesco, G. Barbanti-Bròdano, Assessing the mechanical weakness of vertebrae affected by primary tumors: a feasibility study, Materials 13 (2020) 3256, https://doi.org/10.3390/ma13153256.

[32] V. Danesi, L. Zani, A. Scheele, F. Berra, L. Cristofolini, Reproducible reference frame for in vitro testing of the human vertebrae, J. Biomech. 47 (2014) 313–318, https://doi.org/10.1016/j.jbiomech.2013.10.005.

[33] F. Macedo, K. Ladeira, F. Pinho, N. Saraiva, N. Bonito, L. Pinto, F. Gonçalves, Bone metastases: an overview, Oncol. Rev. (2017), https://doi.org/10.4081/oncol.2017.321.

[34] A.I. Hussein, E.F. Morgan, The effect of intravertebral heterogeneity in microstructure on vertebral strength and failure patterns, Osteoporos. Int. 24 (2013) 979–989, https://doi.org/10.1007/s00198-012-2039-1.

[35] H. Taneichi, K. Kaneda, N. Takeda, K. Abumi, S. Satoh, Risk factors and probability of vertebral body collapse in metastases of the thoracic and lumbar spine:, Spine. 22 (1997) 239–245. doi:https://doi.org/10.1097/00007632-199702010-00002.

[36] E. Dall'Ara, R. Schmidt, D. Pahr, P. Varga, Y. Chevalier, J. Patsch, F. Kainberger, P. Zysset, A nonlinear finite element model validation study based on a novel experimental technique for inducing anterior wedge-shape fractures in human vertebral bodies in vitro, J. Biomech. 43 (2010) 2374–2380, https://doi.org/10.1016/j.jbiomech.2010.04.023.

[37] L.E. Lanyon, Functional strain in bone tissue as an objective and controlling stimulus for adaptive bone remodelling, J. Biomech. 20 (1987) 1093–1098.

[38] C.M. Whyne, S.S. Hu, K.L. Workman, J.C. Lotz, Biphasic material properties of lytic bone metastases, Ann. Biomed. Eng. 28 (2000) 1154–1158, https://doi.org/10.1114/1.1313773.

[39] T.S. Kaneko, J.S. Bell, M.R. Pejcic, J. Tehranzadeh, J.H. Keyak, Mechanical properties, density and quantitative CT scan data of trabecular bone with and without metastases, J. Biomech. 37 (2004) 523–530, https://doi.org/10.1016/j.jbiomech.2003.08.010.

[40] S.K. Eswaran, A. Gupta, M.F. Adams, T.M. Keaveny, Cortical and trabecular load sharing in the human vertebral body, J. Bone Miner. Res. 21 (2005) 307–314, https://doi.org/10.1359/jbmr.2006.21.2.307.

[41] X.-Y. Wang, L.-Y. Dai, H.-Z. Xu, Y.-L. Chi, The load-sharing classification of thoracolumbar fractures: an in vitro biomechanical validation, Spine 32 (2007) 1214–1219, https://doi.org/10.1097/BRS.0b013e318053ec69.

[42] L. Cristofolini, In vitro evidence of the structural optimization of the human skeletal bones, J. Biomech. 48 (2015) 787–796, https://doi.org/10.1016/j.jbiomech.2014.12.010.

[43] L. Cristofolini, N. Brandolini, V. Danesi, M.M. Juszczyk, P. Erani, M. Viceconti, Strain distribution in the lumbar vertebrae under different loading configurations, Spine J. 13 (2013) 1281–1292, https://doi.org/10.1016/j.spinee.2013.06.014.

[44] D. Roodman, Mechanisms of bone metastasis, N. Engl. J. Med. 10 (2004).

[45] J.H. Healey, H.K. Brown, Complications of bone metastases, (n.d.) 12.

[46] C.M. Whyne, Biomechanics of metastatic disease in the vertebral column, Neurol. Res. 36 (2014) 493–501, https://doi.org/10.1179/1743132814Y.0000000362.

[47] D. Weldon, The effects of corticosteroids on bone growth and bone density, Ann. Allergy Asthma Immunol. 103 (2009) 3–11, https://doi.org/10.1016/S1081-1206(10)60135-4.

[48] L. Bollen, K. Groenen, W. Pondaag, C.S.P. van Rijswijk, M. Fiocco, Y.M. Van der Linden, S.P.D. Dijkstra, Clinical evaluation of the spinal instability neoplastic score in patients treated with radiotherapy for symptomatic spinal bone metastases, Spine 42 (2017) E956–E962, https://doi.org/10.1097/BRS.0000000000002058.

[49] M. Palanca, L. Cristofolini, E. Dall'Ara, M. Curto, F. Innocente, V. Danesi, G. Tozzi, Digital volume correlation can be used to estimate local strains in natural and augmented vertebrae: an organ-level study, J. Biomech. 49 (2016) 3882–3890, https://doi.org/10.1016/j.jbiomech.2016.10.018.

[50] A. Isaac, D. Dalili, D. Dalili, M.-A. Weber, State-of-the-art imaging for diagnosis of metastatic bone disease, Radiology (2020), https://doi.org/10.1007/s00117-020-00666-6.

[51] S. Boriani, J.N. Weinstein, R. Biagini, Primary bone tumors of the spine, terminology and surgical staging, Spine 22 (1997) 1036–1044.

[52] W. Enneking, S. Spanier, M. Goodman, A system for the surgical staging of musculoskeletal sarcoma, Clin. Orthop. (1980) 15.

[53] A.G. Bruno, K. Burkhart, B. Allaire, D.E. Anderson, M.L. Bouxsein, Spinal loading patterns from biomechanical modeling explain the high incidence of vertebral fractures in the thoracolumbar region: biomechanical modeling of spinal loading patterns, J. Bone Miner. Res. 32 (2017) 1282–1290, https://doi.org/10.1002/jbmr.3113.